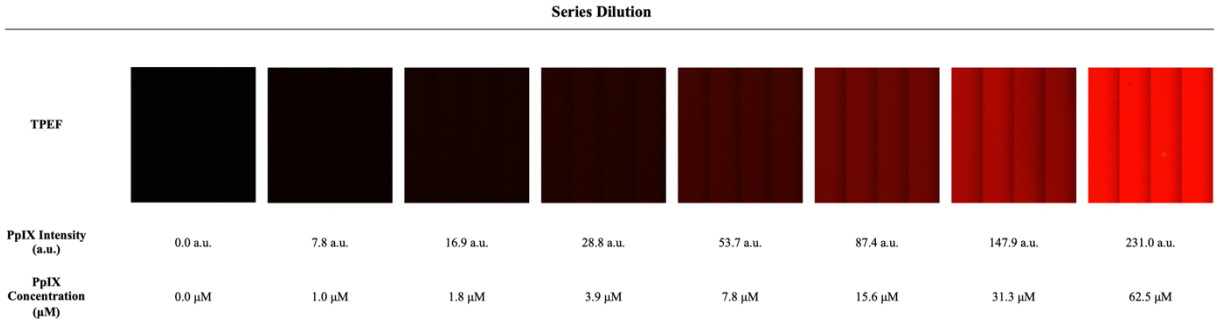

Supplementary Fig. 1 | TPEF imaging of serial dilutions of PpIX. Serial dilutions of PpIX ranging from 0 to 62.5 micrograms/mL were imaged with TPEF imaging. The measured fluorescence intensity of the PpIX serial dilutions shows a direct relationship between fluorescence intensity and PpIX concentration.

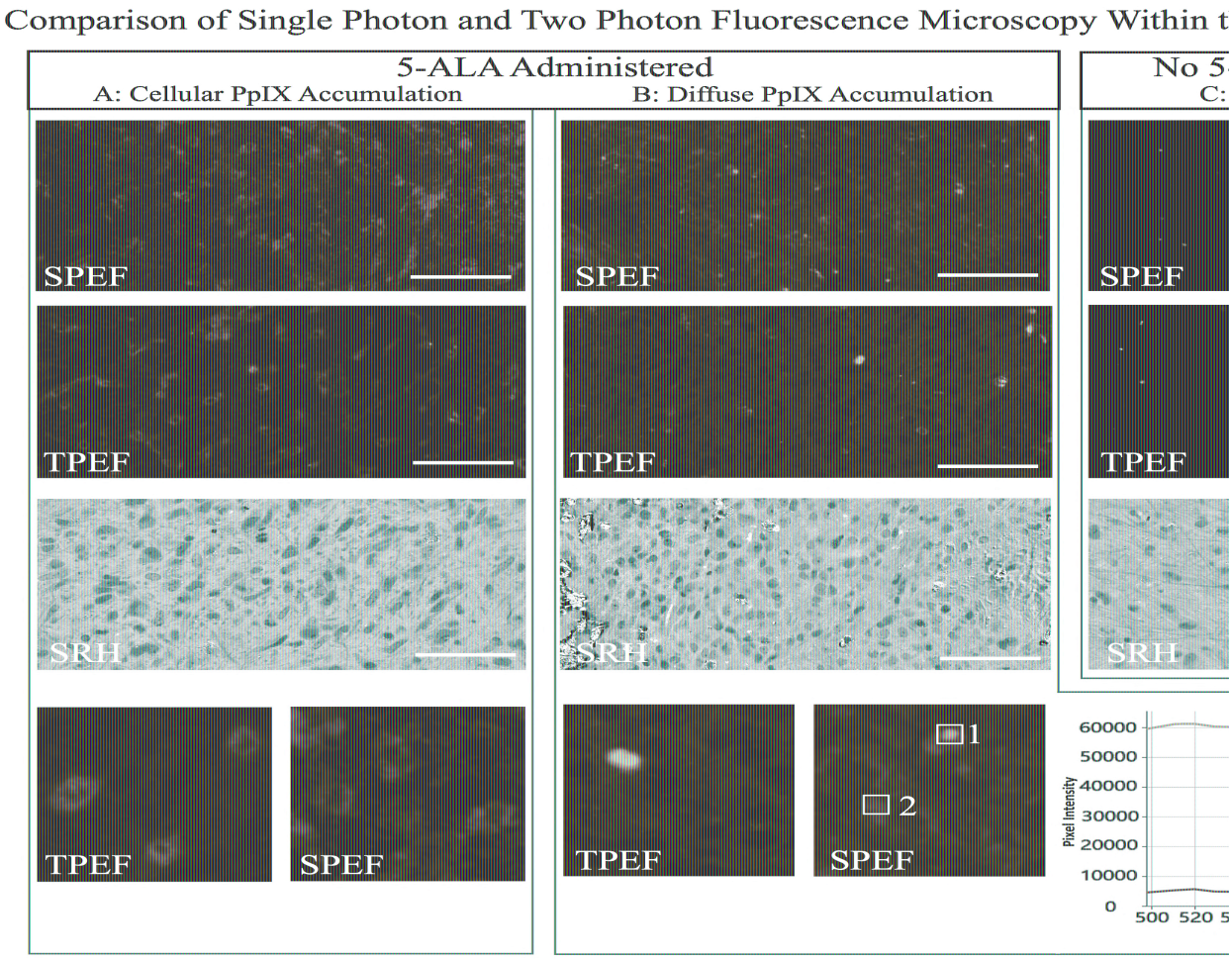

Supplementary Fig. 2 | SPEF/TPEF. Surgical specimens from 6 glioblastoma patients treated with 5-ALA and one control were collected and evenly divided for imaging with SPEF (Zeiss LSM 880) and TPEF (NIO Imaging system). Each panel labeled SPEF is created by overlaying the 636nm emission channel (PpIX) with the 564nm emission channel (autofluorescence). Panel A demonstrates an example of PpIX accumulation in a cellular pattern as imaged with SPEF and TPEF. SRH reveals that a limited fraction of imaged cells concentrate PpIX in the cytoplasm. High magnification field of view (73x73 microns) reveals bright cytoplasmic signal with dark nuclei indicating cytoplasmic accumulation of PpIX. Panel B demonstrates a diffuse dim pattern of PpIX accumulation with largely homogenous accumulation of PpIX in the imaged tissue. There are some intensely fluorescence structures in both the SPEF and TPEF images. A multispectral analysis of representative regions labeled 1 and 2 demonstrate the spectral differences. Region 1 demonstrates fluorescence intensity that is uniform from 500-580nm with a gradual decay as the emission is measured towards the infrared end of the spectrum. Region 2 demonstrates peak emission at 636nm in a pattern that is characteristic of PpIX. Demonstrating the appearance of tissue when 5-ALA is not administered, panel C reveals a modest degree of speckle fluorescence without appreciable signal at 636nm.

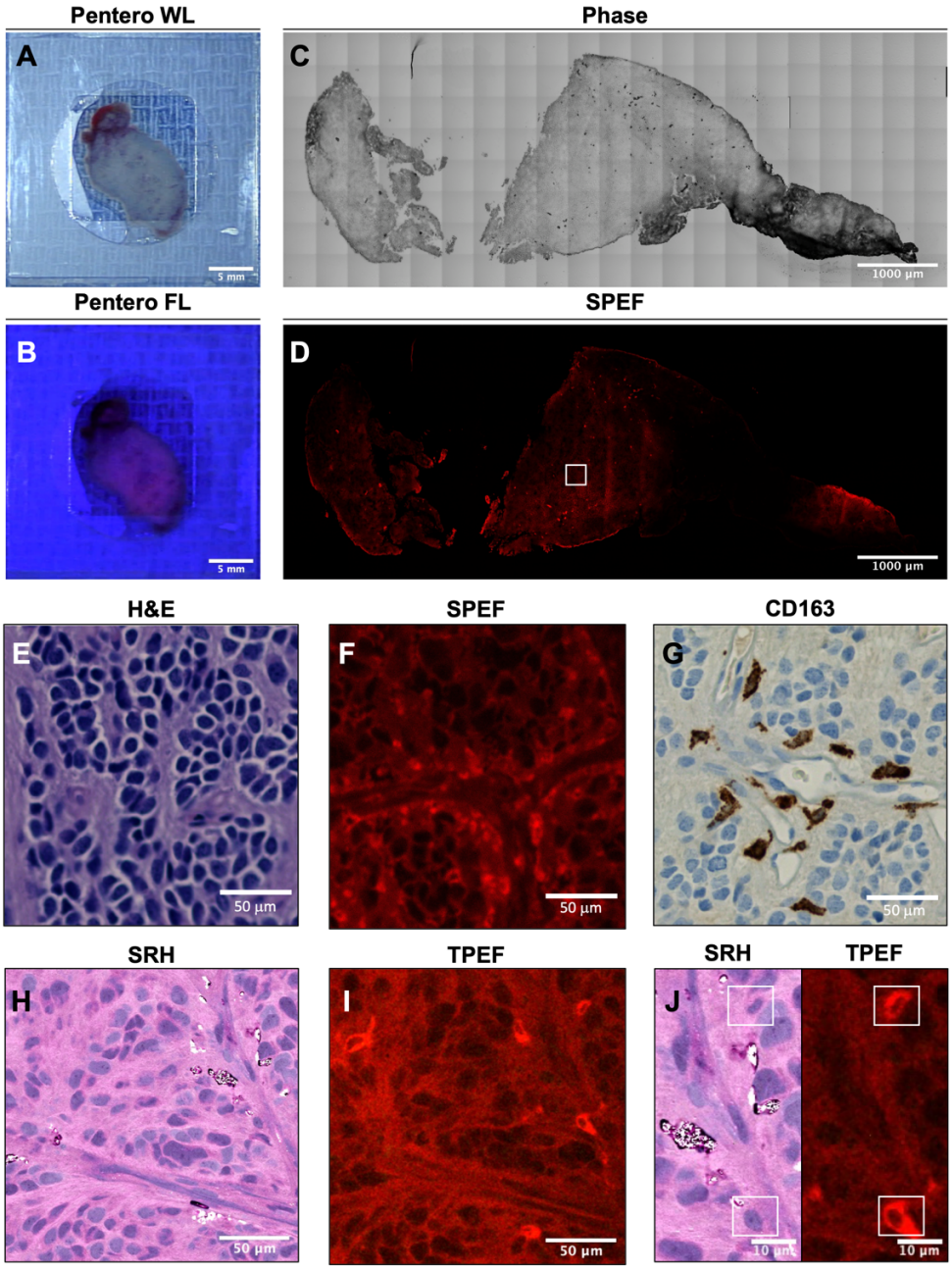

Supplementary Fig. 3 | Comparison of SPEF and TPEF. A fluorescing tumor specimen was viewed with white light (WL) (a) and blue light (b) under the Zeiss Pentero surgical microscope in the operating room (patient 45). A cryosection from the same specimen was created and imaged with phase-contrast microscopy (c) and single photon excitation fluorescence microscopy (d). The section was stained with H&E and shows a high density of tumor cells (e). A small subset of cells accumulate PpIX within the cytoplasm in the section imaged with single photon microscopy (f). A section stained with CD163 demonstrates a similar density of positive cells when compared to fluorescing cells in (f). SRH imaging of the same specimen (h) shows highly dense tumor with morphology mirroring the H&E section (d). Two-photon excitation fluorescence microscopy of the specimen also shows a small subset of cells with PpIX accumulation in the cytoplasm consistent with (f) and (g). High magnification comparison of SRH and TPEF imaging reveals that cells with cytoplasmic accumulation of PpIX are morphologically similar to histiocytes in (g).

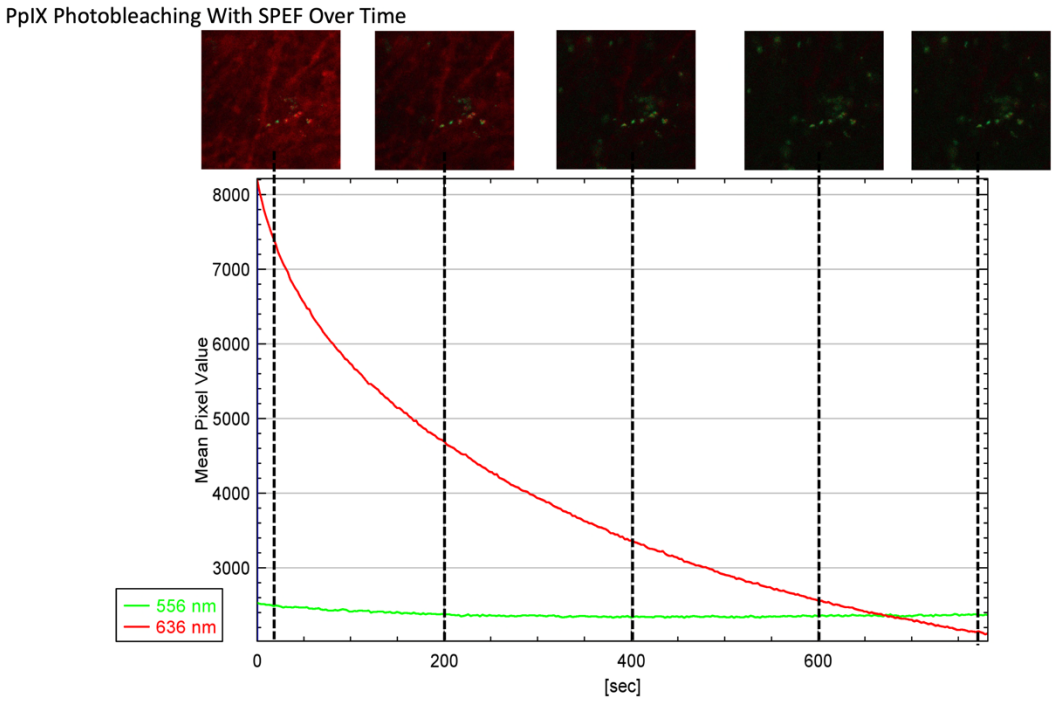

Supplementary Fig. 4 | Photobleaching of PpIX with SPEF imaging. Unprocessed tissue from a 5-ALA-treated GBM patient was subjected to a photobleaching experiment demonstrated here. Laser focus was established in the field of view shown and the tissue was exposed to 405nm excitation over 13 minutes. Over time the 636nm signal characteristic of PpIX decays in an exponential fashion while the 556nm signal, characteristic of autofluorescence, remains constant over time.

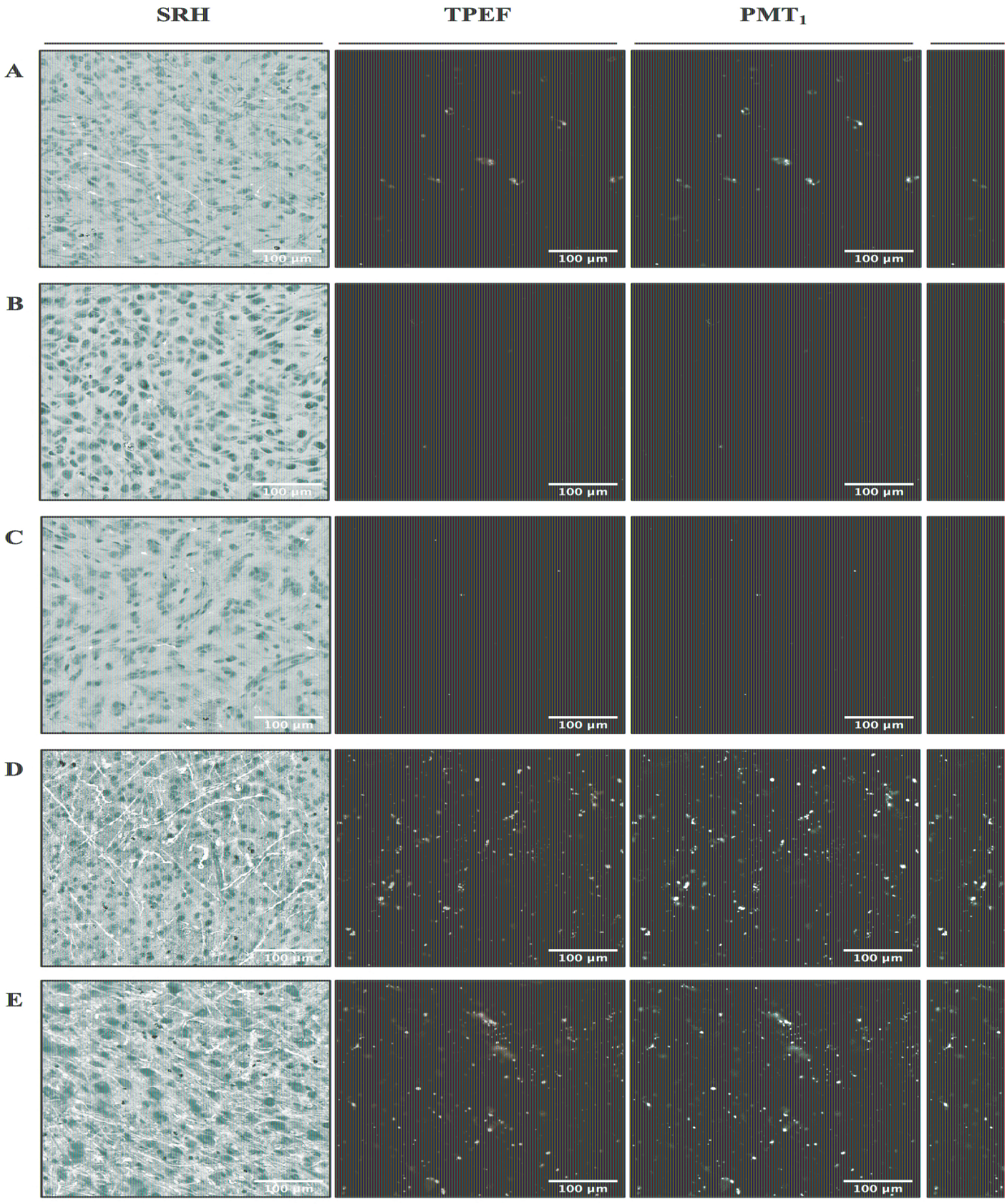

Supplementary Fig. 5 l Paired SRH/TPEF imaging in high grade glioma patients who did not receive 5-ALA. These negative control SRH/TPEF image pairs demonstrate a variable degree of autofluorescence where signal is present in both PMT1 and PMT2 channels in the absence of PMT1-specific signal. (a, patient 71; b, patient 72; c, patient 73; d, patient 74; e, patient 75).

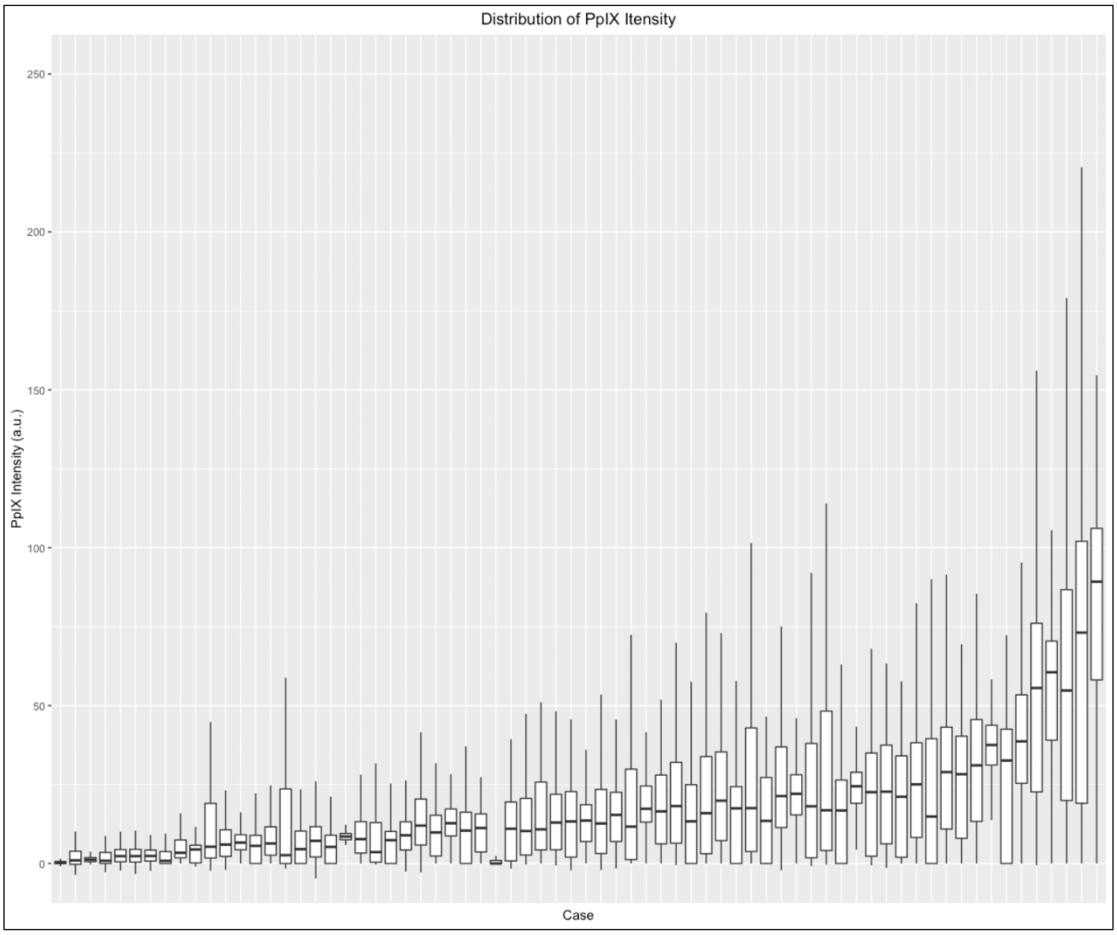

Supplementary Fig. 6 l Distribution of PpIX intensity across each patient's imaged field of views. The boxplot for each patient demonstrates the variation of PpIX accumulation and intensity within and between patients. Each box ranges from the first quartile to the third quartile of the distribution and the median is marked by a line across the box. The lines extending from each box represent $\pm 1.5 \times interquartile\ range$.

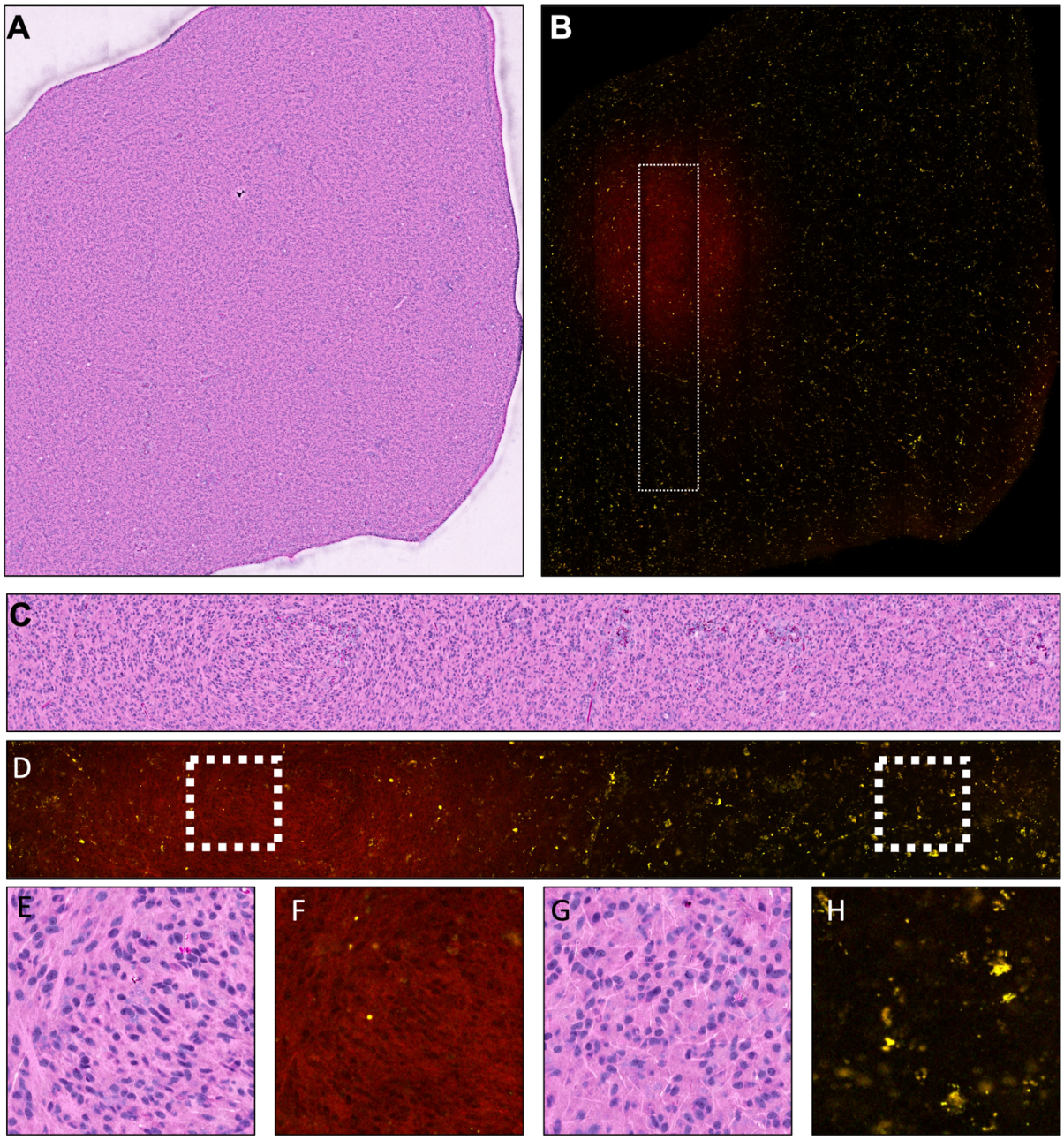

Supplementary Fig. 7 | Intra-specimen variation of PpIX accumulation. SRH/TPEF imaging reveals the heterogeneity of PpIX accumulation within a given specimen of consistent cellular density. (a) SRH imaging reveals a highly cellular tumor specimen. (b) TPEF imaging reveals that the tumor specimen contains a weak autofluorescence throughout with a small focus of PpIX accumulation. (c) A strip of the SRH imaging reveals the cellular density is consistent throughout. (d) A strip of TPEF imaging of the same area reveals that the transition from diffuse bright PpIX fluorescence to diffuse dim PpIX fluorescence to autofluorescence. (e) SRH imaging of the diffuse bright region shows highly cellular tumor. (f) TPEF imaging reveals diffuse bright fluorescence. (g) SRH imaging of the autofluorescence region shows cellular density equivalent to that in E. (h) TPEF imaging reveals autofluorescence.

AXONAL PPIX ACCUMULATION ATLAS

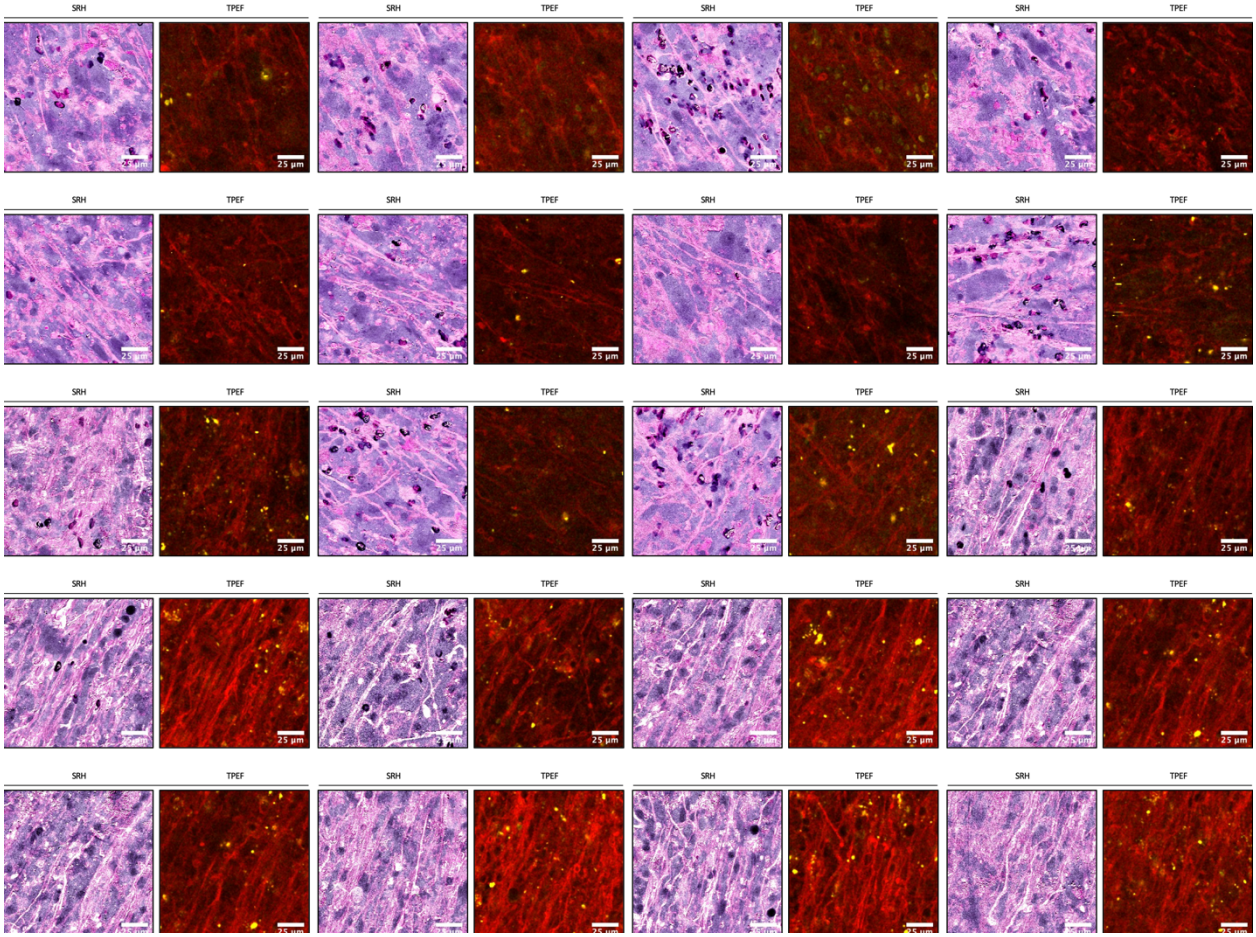

Supplementary Fig. 8 | Atlas of axonal accumulation of PpIX. Axonal accumulation of PpIX is readily apparent and marked by linear structures with strong PMT-1 signal in the 20 shown fields of view. Axonal accumulation was present in 935 of 166,743) fields of view across the study.

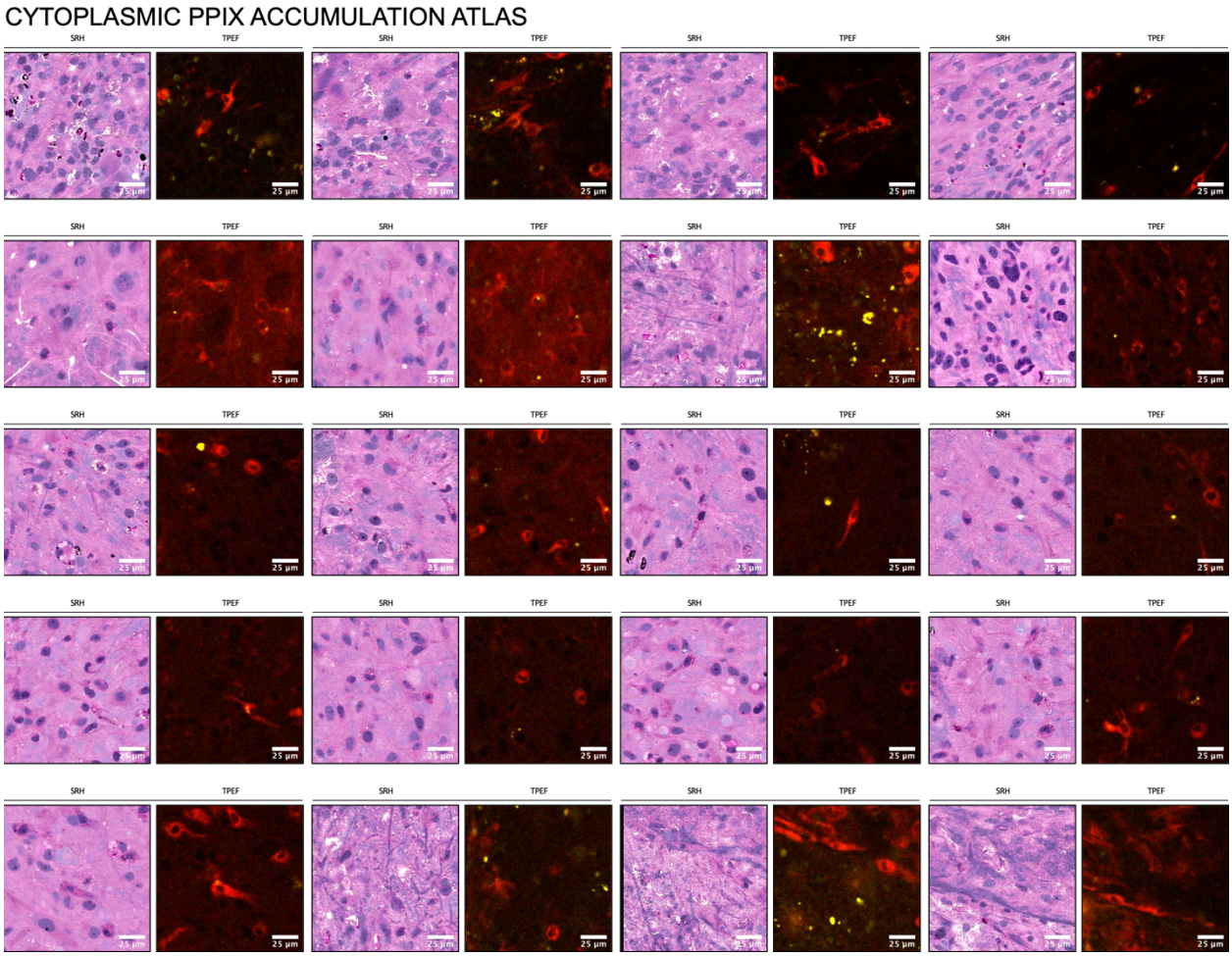

Supplementary Fig. 9 | Atlas of cytoplasmic accumulation of PpIX. Cytoplasmic accumulation of PpIX is focally present in a subset of cells amongst imaged specimens. 20 prototypic examples of cytoplasmic accumulation of PPIX are shown here. Cytoplasmic accumulation was present in 19,057 of 166,743 fields of view collected in this study.

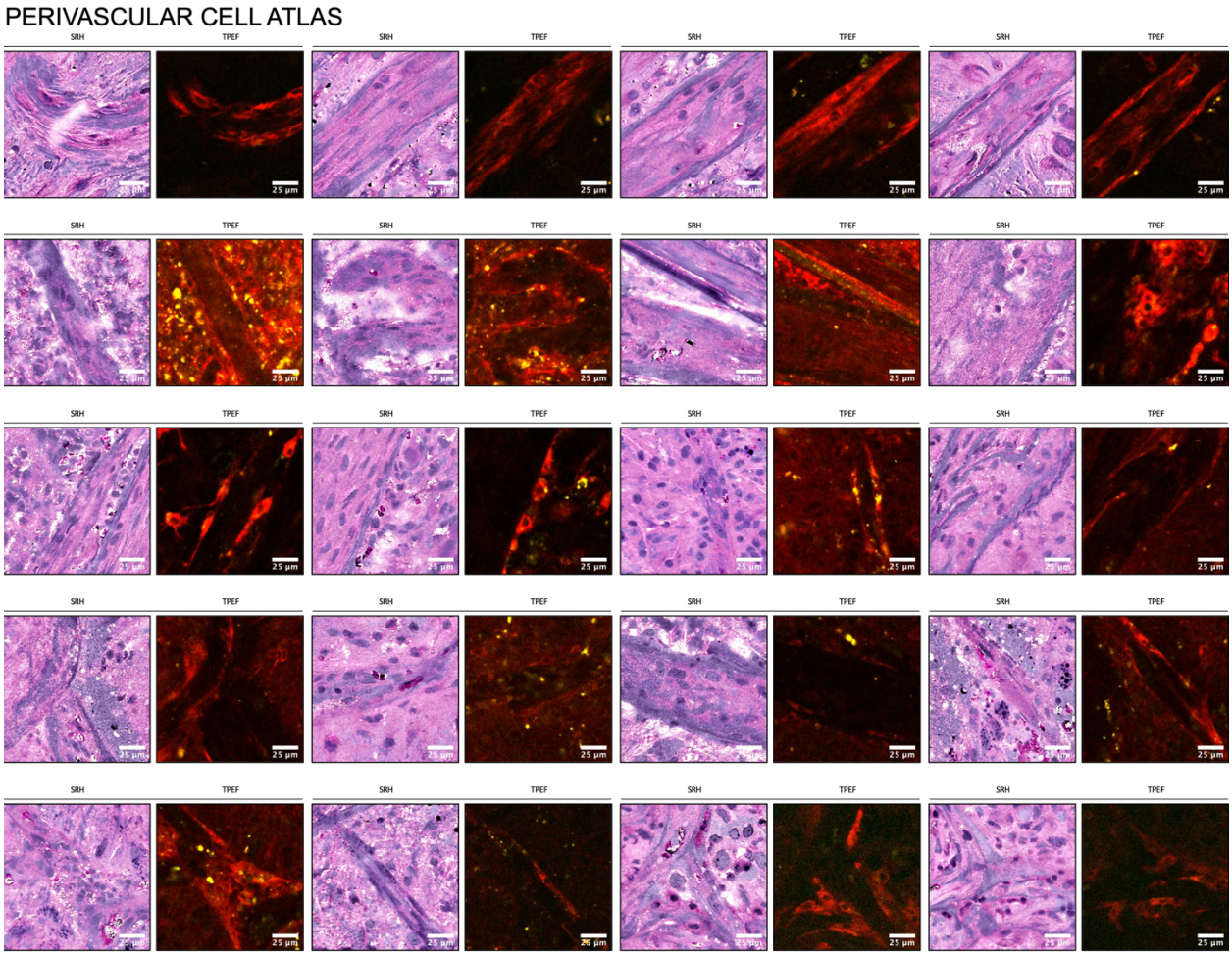

Supplementary Fig. 10 | Atlas of perivascular cytoplasmic accumulation of PpIX. Cytoplasmic accumulation of PpIX is focally present in a subset of cells with a strong PMT-1 signal and that are close to blood vessels. Cytoplasmic accumulation is present in 510 of 166,743 fields of view.

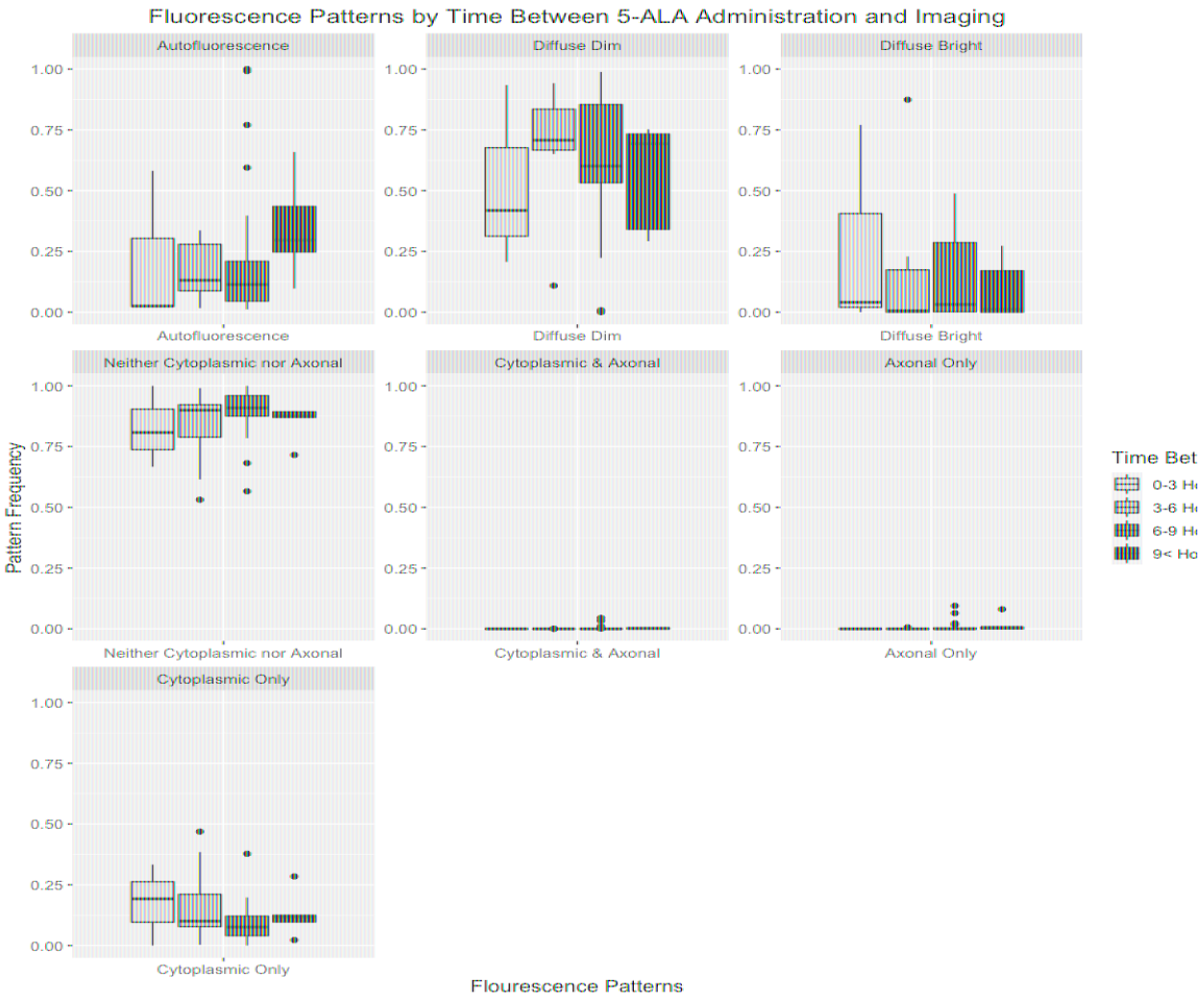

Supplementary Fig. 11 Frequency of fluorescence patterns by time between 5-ALA administration and TPEF Imaging. The boxplots shown for each fluorescence pattern demonstrates the variation in the proportion of FOVs demonstrating the given fluorescence pattern in the given time window between 5-ALA administration and TPEF imaging. Each box ranges from the first quartile to the third quartile of the distribution and the median is marked by a line across the box. The lines extending from each box represent ±1.5 × $interquartile\ range$.

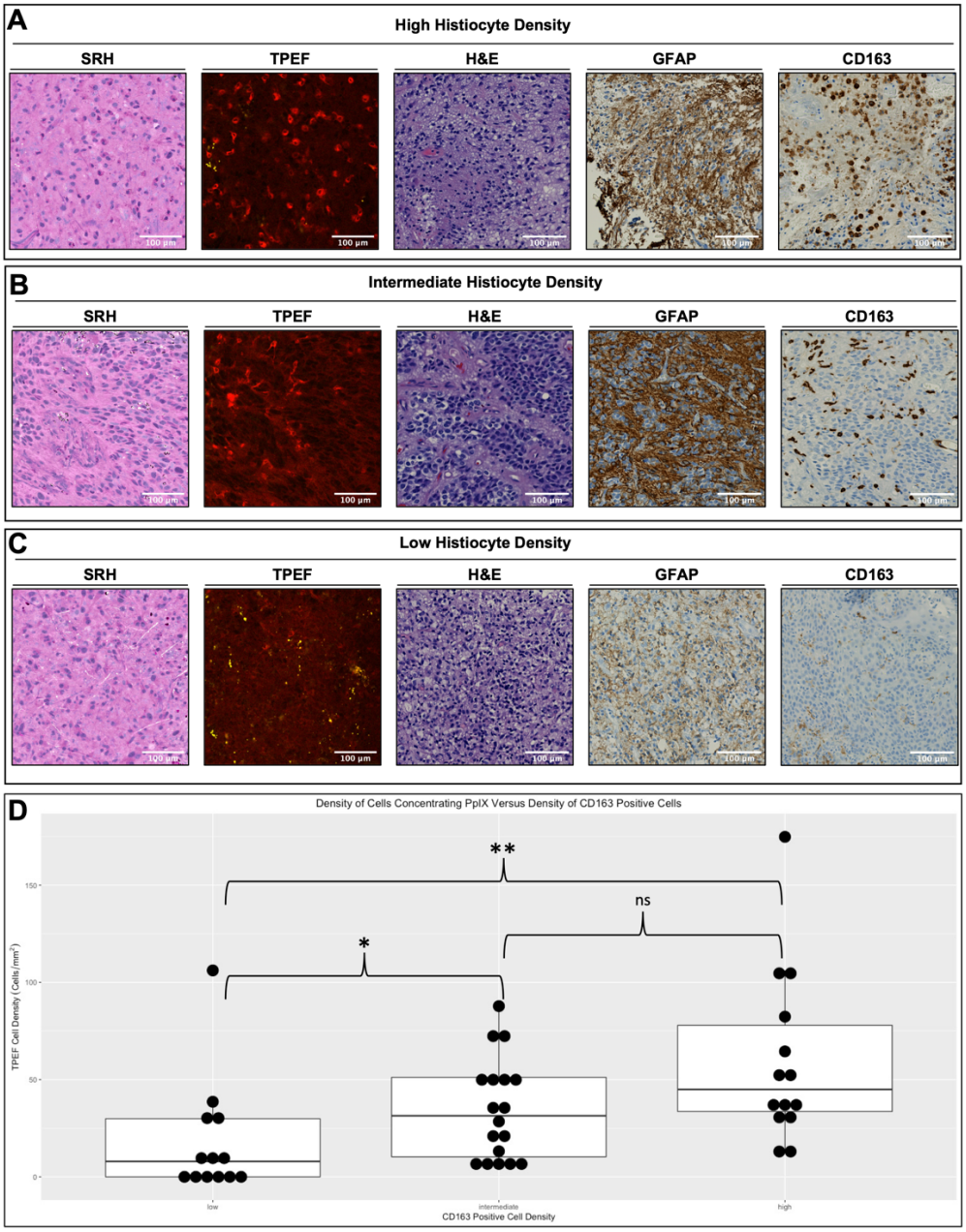

Supplementary Fig. 12 | Relationship between cellular accumulation of PpIX and abundance of histiocytes. A range of histiocyte density was encountered in the 70 patients enrolled. Specimens revealing hypercellular pleomorphic, high-grade glial neoplasms on SRH and conventional H&E reveal variations in the abundance of CD163 positive cells that correlate qualitatively with the abundance of cells with PpiX concentrated within the cytoplasm. Examples of high histiocyte density (a, patient 32), intermediate histiocyte density (b, patient 45) and low histiocyte density (c, patient 42) are shown here. The association of CD163 positivity and the number of cells with high PpIX cytoplasmic concentration is demonstrated in the study subjects with tissue available for CD163 staining (d, n=45). Cells concentrating PpIX in the cytoplasm were more abundant in specimens with intermediate (*: p=0.02) and high CD163 positivity (**: p=0.002) though there was no significant difference between PpIX cellularity comparing specimens with intermediate versus high CD163 positivity (n.s.: no statistical significance, p=0.06). Each box ranges from the first quartile to the third quartile of the distribution and the median is marked by a line across the box. The lines extending from each box represent ±1.5×interquartile range.

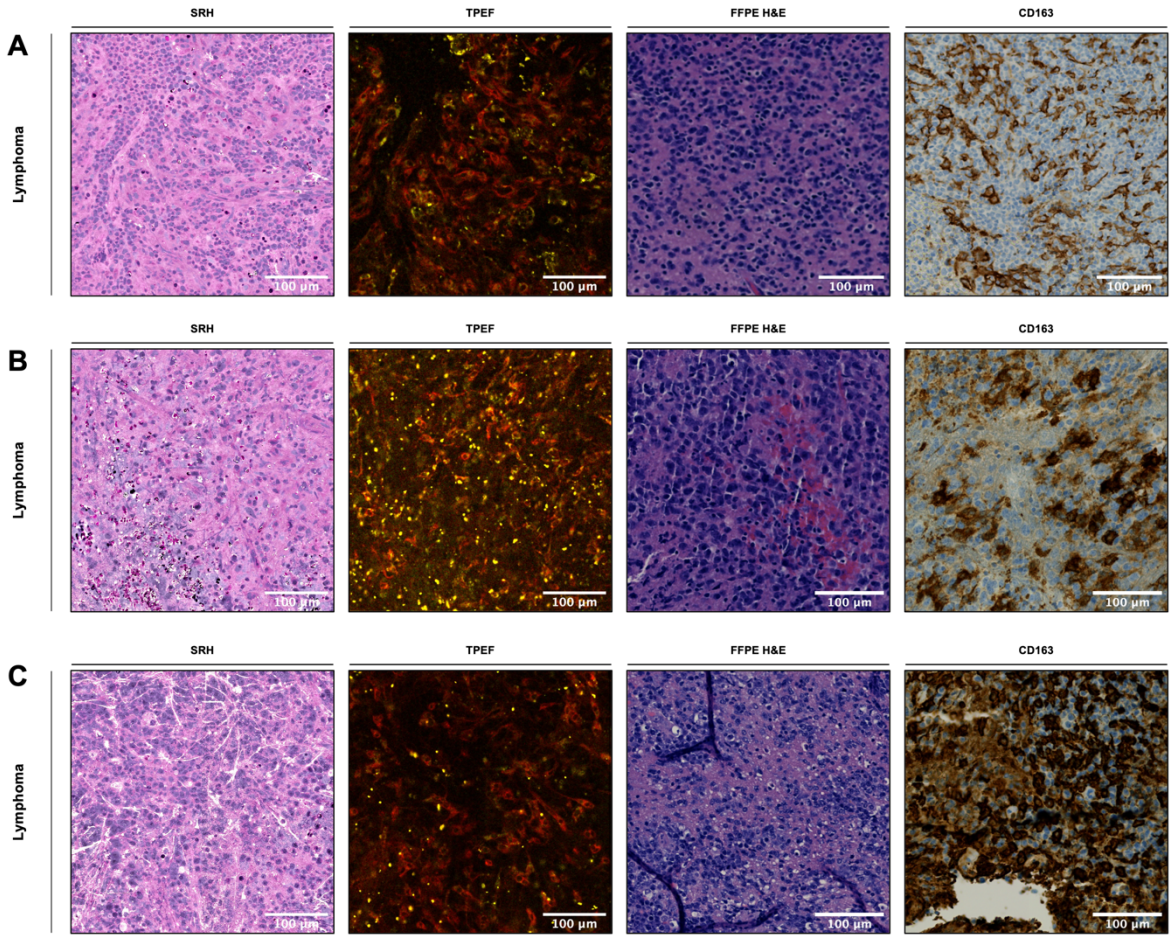

Supplementary Fig. 13 | CD163 staining in lymphoma patients. Cells accumulating PpIX in lymphoma specimens are morphologically consistent with those histiocytes present in high grade glioma specimens. Immunohistochemistry on the same specimens revealed CD163 positive cells with similar abundance to the PpIX accumulating cells in each of the three patients (a, patient 76; b, patient 77; c, Patient 78).

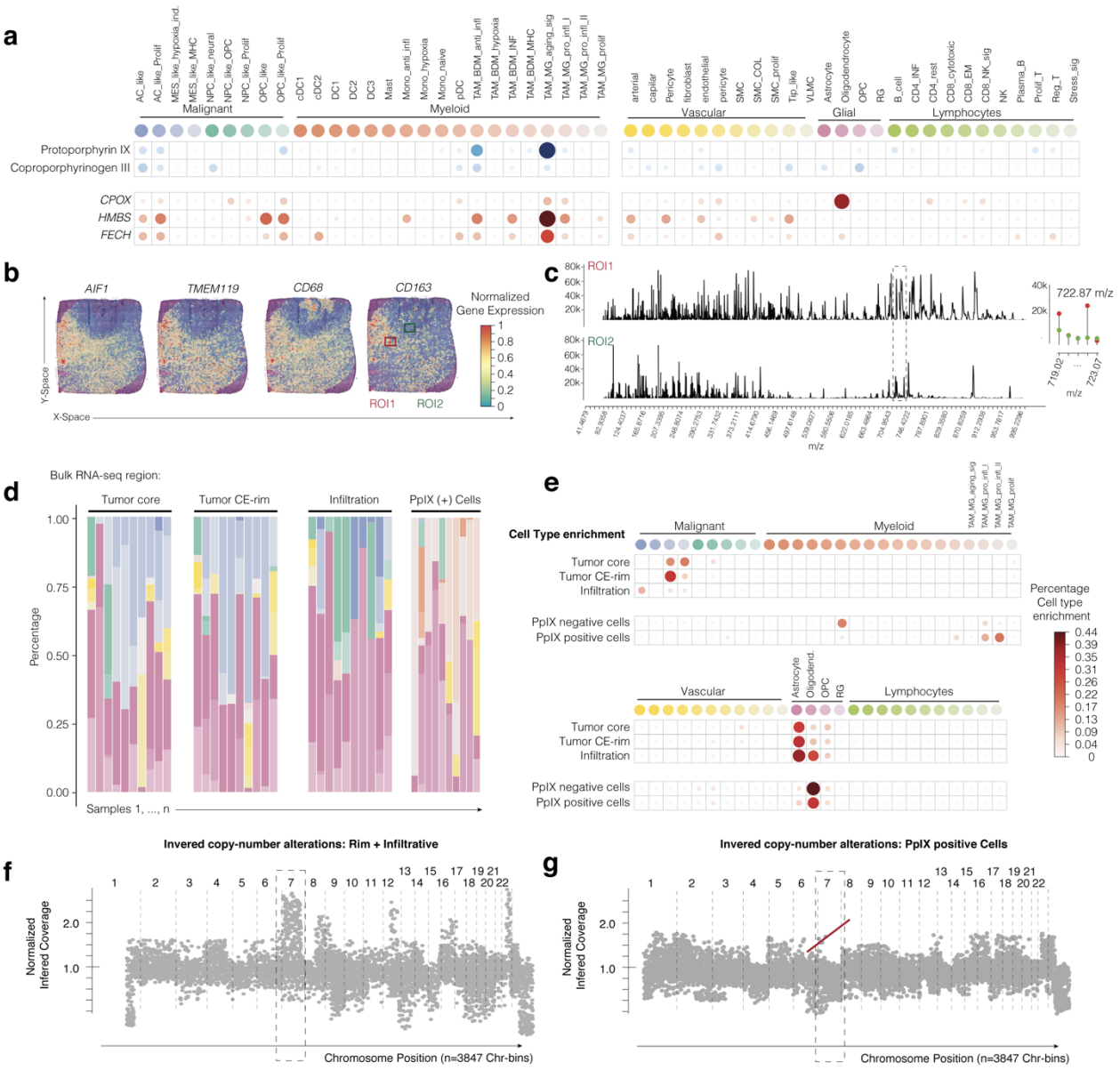

Supplementary Fig. 14 | Additional Transcriptomic and metabolomic analysis of PpIX accumulating cells. The spatially weighted correlation analysis of enzymes (red) and metabolites (blue) with cell type likelihood scores in six patients is displayed in the dot plot (**a**). The surface plot of myeloid gene expression is shown in (**b**). Mass spectra of selected ROIs (left) with high resolution of the PpIX peak at 722.6m/z are shown in (**c**). The cell composition of the bulk RNA-sequencing data is shown in the stacked bar graph (**d**). The percentage of cell type enrichment is shown in (**e**). The derived copy number profiles using SPATA2 toolbox for infiltrative tumor are shown in (**f**) and that for PpIX positive cells are shown in (**g**).

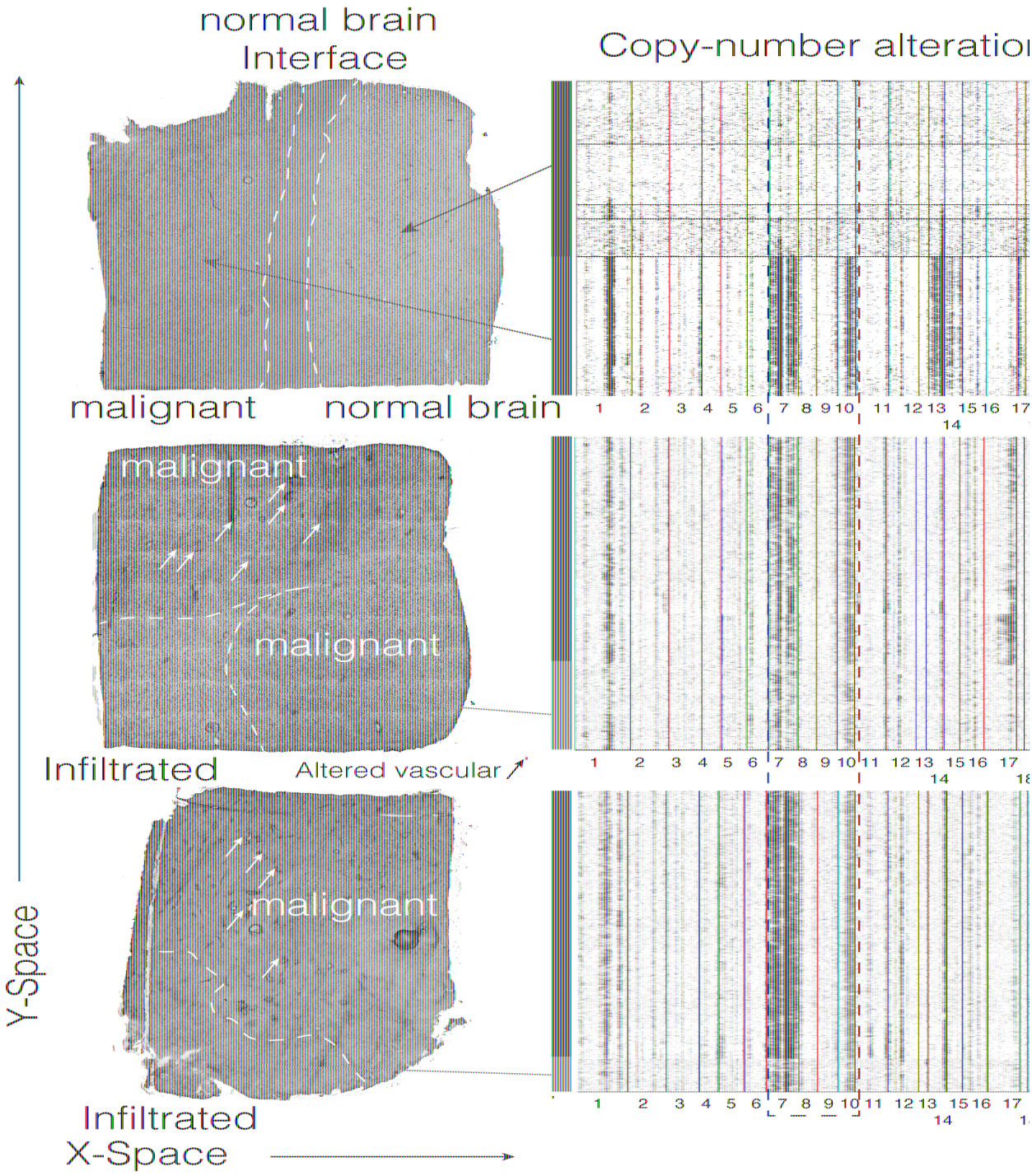

Supplementary Fig. 15 | Copy Number Analysis of Tumor Sample. On the left: H&E images of representative patients with distinct histological features. The arrows point to areas of vascular proliferation. On the right: heatmaps of the inferred copy number alterations (red: chromosome gain, blue: chromosome loss) of the representative samples. CNA analysis confirms the malignant and non-malignant parts of the sample. The color code on the CNA maps: red: malignant, orange: intermediate, green: infiltrative/normal.

Patient	Institution	Age	Final Diagnosis	Grade	WHO Molecular Information	Recurrent	Enhancement Pattern
1	Muenster	71	Glioblastoma	IV	IDH wildtype	No	Necrotic ring
2	Muenster	58	Glioblastoma	IV	IDH wildtype	Yes	Heterogeneous
3	Muenster	50	Glioblastoma	IV	IDH wildtype	Yes	Necrotic ring
4	Muenster	43	Glioblastoma	IV	IDH wildtype	No	Heterogeneous
5	Muenster	64	Glioblastoma	IV	IDH wildtype	Yes	Nodular
6	Muenster	55	Glioblastoma	IV	IDH wildtype	Yes	Heterogeneous
7	Muenster	72	Glioblastoma	IV	IDH wildtype	Yes	Necrotic ring
8	NYU	25	Glioblastoma	IV	IDH wildtype	No	Heterogeneous
9	NYU	61	Glioblastoma	IV	IDH wildtype	No	Nodular
10	NYU	54	Anaplastic astrocytoma	III	IDH wildtype	No	Heterogeneous
11	NYU	54	Glioblastoma	IV	IDH wildtype	No	Necrotic ring
12	NYU	53	Glioblastoma	IV	IDH wildtype	No	Heterogeneous
13	NYU	71	Glioblastoma	IV	IDH wildtype	No	Necrotic ring
14	NYU	54	Glioblastoma	IV	IDH wildtype	No	Necrotic ring
15	NYU	53	Glioblastoma	IV	IDH wildtype; 1p intact, 19q loss	No	Necrotic ring
16	NYU	67	Glioblastoma	IV	IDH wildtype	No	Necrotic ring
17	NYU	54	Glioblastoma	IV	IDH wildtype	No	Homogeneous
18	NYU	62	Glioblastoma	IV	IDH wildtype	No	Necrotic ring
19	NYU	42	Glioblastoma	IV	IDH wildtype	No	Necrotic ring
20	NYU	74	Glioblastoma	IV	IDH wildtype	No	Necrotic ring
21	NYU	63	Glioblastoma	IV	IDH wildtype	No	Heterogeneous
22	NYU	27	High grade glioma	High grade	IDH wildtype, 1p19q intact	No	Necrotic ring
23	NYU	48	Glioblastoma	IV	IDH wildtype, 1p19q intact	No	Necrotic ring
24	NYU	33	Glioblastoma	IV	IDH wildtype	No	Necrotic ring
25	NYU	69	Glioblastoma	IV	IDH wildtype	No	Necrotic ring
26	NYU	46	Glioblastoma	IV	IDH wildtype; 1p intact, 19q loss	No	Necrotic ring
27	NYU	52	Glioblastoma	IV	IDH wildtype	No	Necrotic ring
28	NYU	58	Glioblastoma	IV	IDH wildtype	No	Necrotic ring
29	NYU	73	Glioblastoma	IV	IDH wildtype, 1p19q intact	No	Necrotic ring
30	NYU	54	Glioblastoma	IV	IDH wildtype, 1p19q intact	No	Necrotic ring
31	NYU	59	Glioblastoma	IV	IDH wildtype	No	Necrotic ring
32	NYU	54	Glioblastoma	IV	IDH wildtype	No	Necrotic ring
33	NYU	46	Glioblastoma	IV	IDH wildtype, 1p19q intact	Yes	Heterogeneous
34	NYU	76	Glioblastoma	IV	IDH wildtype	No	Nodular
35	NYU	74	Glioblastoma	IV	IDH wildtype	No	Necrotic ring
36	NYU	52	Glioblastoma	IV	IDH wildtype, 1p19q intact	No	Necrotic ring
37	NYU	65	Glioblastoma	IV	IDH wildtype	No	Homogeneous
38	NYU	85	Glioblastoma	IV	IDH wildtype	No	Heterogeneous
39	NYU	65	Glioblastoma	IV	IDH wildtype	No	Homogeneous
40	NYU	64	Glioblastoma	IV	IDH wildtype, 1p19q intact	No	Necrotic ring
41	NYU	70	Glioblastoma	IV	IDH wildtype	No	Necrotic ring
42	NYU	55	Glioblastoma	IV	IDH wildtype	No	Necrotic ring
43	NYU	46	Glioblastoma	IV	IDH wildtype	Yes	Necrotic ring
44	NYU	73	Glioblastoma	IV	IDH wildtype, 1p19q intact	No	Necrotic ring
45	NYU	18	Anaplastic neuroepithelial tumor	N/A	IDH wildtype	No	Heterogeneous
46	NYU	27	Astrocytoma	IV	IDH mutated	No	Nodular
47	NYU	50	Glioblastoma	IV	IDH wildtype	No	Necrotic ring
48	NYU	49	Glioblastoma	IV	IDH wildtype; 1p intact, 19q loss	No	Heterogeneous
49	NYU	68	Glioblastoma	IV	IDH wildtype	No	Necrotic ring
50	NYU	52	Glioblastoma	IV	IDH wildtype	No	Heterogeneous
51	NYU	41	Astrocytoma	IV	IDH mutated, 1p19q intact	No	Heterogeneous
52	NYU	35	Astrocytoma	IV	IDH wildtype, 1p19q intact	No	Homogeneous
53	NYU	54	Glioblastoma	IV	IDH wildtype	No	Necrotic ring
54	Vienna	70	Glioblastoma	IV	IDH wildtype	Yes	Necrotic ring
55	Vienna	27	Glioblastoma	IV	IDH mutated	Yes	Necrotic ring
56	Vienna	67	Glioblastoma	IV	IDH wildtype	No	Necrotic ring
57	Vienna	80	Glioblastoma	IV	IDH wildtype	No	Necrotic ring
58	Vienna	43	Anaplastic Astrocytoma	III	IDH mutated	No	Heterogeneous
59	Vienna	73	Glioblastoma	IV	IDH wildtype	No	Necrotic ring
60	Vienna	56	Glioblastoma	IV	IDH wildtype	Yes	Necrotic ring
61	Vienna	52	Glioblastoma	IV	IDH wildtype	No	Necrotic ring
62	Vienna	42	Glioblastoma	IV	IDH wildtype	No	Necrotic ring
63	Vienna	72	Glioblastoma	IV	IDH wildtype	No	Necrotic ring
64	Vienna	56	Glioblastoma	IV	IDH wildtype	No	Necrotic ring
65	Vienna	51	Glioblastoma	IV	IDH wildtype	Yes	Necrotic ring
66	Vienna	68	Glioblastoma	IV	IDH wildtype	No	Necrotic ring
67	Vienna	49	Glioblastoma	IV	IDH wildtype	No	Necrotic ring
68	Vienna	59	Glioblastoma	IV	IDH wildtype	No	Necrotic ring
69	Vienna	38	Glioblastoma	IV	IDH wildtype	No	Necrotic ring
70	Vienna	59	Glioblastoma	IV	IDH mutated	No	Necrotic ring
71	NYU	27	Anaplastic Oligodendroglioma	III	Mutant	Co-deleted	N/A
72	NYU	52	Anaplastic Oligodendroglioma	III	Mutant	Co-deleted	N/A
73	NYU	73	Glioblastoma	IV	Wild Type	Not performed	N/A
74	NYU	49	Oligodendroglioma	III	Mutant	Co-deleted	N/A
75	NYU	54	Glioblastoma	IV	Wild Type	Not performed	N/A
76	NYU	53	Lymphoma	N/A	N/A	No	N/A
77	NYU	76	Lymphoma	N/A	N/A	No	N/A
78	NYU	77	Lymphoma	N/A	N/A	No	N/A

Supplementary Table 1 | Diagnostic information for study patients.

Effect	Estimate	Std. Error	t value	Pr(>|t|)	Significance
Intercept	3.98701	1.13514	3.512	0.00112	*
Time between 5-ALA administration and Imaging (hours)	-0.09708	0.11843	-0.82	0.41723	ns
Ki-67 Proliferation Index	0.70876	1.59792	0.444	0.65976	ns
Homogeneous Enhancing Pattern	-1.19725	1.22103	-0.981	0.33272	ns
Necrotic Ring Enhancing Pattern	0.59407	0.63836	0.931	0.35763	ns
Nodular Enhancing Pattern	0.94346	0.97506	0.968	0.33906	ns
Proportion of Enhancing Tumor	-2.27917	1.53576	-1.484	0.14563	ns

Supplementary Table 2 | Fixed effects analysis of PpIX concentration in patient specimens.

Supplementary Video 1 | Pan/zoom around tissue with high cellularity and autofluorescence.
YouTube

Supplementary Video 2 | Pan/zoom around tissue with high cellularity and diffuse dim PpIX fluorescence.
YouTube

Supplementary Video 3 | Pan/zoom around tissue with high cellularity and diffuse bright PpIX fluorescence.
YouTube

Supplementary Video 4 | Pan/zoom around tissue with high cellularity and diffuse dim PpIX fluorescence with cells concentrating PPIX.
YouTube

Supplementary Video 5 | Pan/zoom around tissue with axonal accumulation of PpIX.
YouTube